Diagnosing implosion performance at the National Ignition Facility (NIF) by means of neutron spectrometry

2013 Nucl. Fusion 53 043014

(http://iopscience.iop.org/0029-5515/53/4/043014)

Nucl. Fusion **53** (2013) 043014 (8pp) doi:10.1088/0029-5515/53/4/043014

Diagnosing implosion performance at the National Ignition Facility (NIF) by means of neutron spectrometry

J.A. Frenje[1], R. Bionta[2], E.J. Bond[2], J.A. Caggiano[2], D.T. Casey[1], C. Cerjan[2], J. Edwards[2], M. Eckart[2], D.N. Fittinghoff[2], S. Friedrich[2], V.Yu. Glebov[3], S. Glenzer[2], G. Grim[6], S. Haan[2], R. Hatarik[2], S. Hatchett[2], M. Gatu Johnson[1], O.S. Jones[2], J.D. Kilkenny[4], J.P. Knauer[3], O. Landen[2], R. Leeper[5], S. Le Pape[2], R. Lerche[2], C.K. Li[1], A. Mackinnon[2], J. McNaney[2], F.E. Merrill[6], M. Moran[2], D.H. Munro[2], T.J. Murphy[6], R.D. Petrasso[1], R. Rygg[2], T.C. Sangster[3], F.H. Séguin[1], S. Sepke[2], B. Spears[2], P. Springer[2], C. Stoeckl[3] and D.C. Wilson[6]

[1] Massachusetts Institute of Technology, Cambridge, MA 02139, USA
[2] Lawrence Livermore National Laboratory, Livermore, CA 94550, USA
[3] Laboratory for Laser Energetics, University of Rochester, Rochester, NY 14623, USA
[4] General Atomics, San Diego, CA 92186, USA
[5] Sandia National Laboratory, NM, 87123, USA
[6] Los Alamos National Laboratory, NM, 87545, USA

Received 13 November 2012, accepted for publication 5 March 2013
Published 28 March 2013
Online at stacks.iop.org/NF/53/043014

Abstract
The neutron spectrum from a cryogenically layered deuterium–tritium (dt) implosion at the National Ignition Facility (NIF) provides essential information about the implosion performance. From the measured primary-neutron spectrum (13–15 MeV), yield (Y_n) and hot-spot ion temperature (T_i) are determined. From the scattered neutron yield (10–12 MeV) relative to Y_n, the down-scatter ratio, and the fuel areal density (ρR) are determined. These implosion parameters have been diagnosed to an unprecedented accuracy with a suite of neutron-time-of-flight spectrometers and a magnetic recoil spectrometer implemented in various locations around the NIF target chamber. This provides good implosion coverage and excellent measurement complementarity required for reliable measurements of Y_n, T_i and ρR, in addition to ρR asymmetries. The data indicate that the implosion performance, characterized by the experimental ignition threshold factor, has improved almost two orders of magnitude since the first shot taken in September 2010. ρR values greater than $1\,g\,cm^{-2}$ are readily achieved. Three-dimensional semi-analytical modelling and numerical simulations of the neutron-spectrometry data, as well as other data for the hot spot and main fuel, indicate that a maximum hot-spot pressure of ~150 Gbar has been obtained, which is almost a factor of two from the conditions required for ignition according to simulations. Observed Y_n are also 3–10 times lower than predicted. The conjecture is that the observed pressure and Y_n deficits are partly explained by substantial low-mode ρR asymmetries, which may cause inefficient conversion of shell kinetic energy to hot-spot thermal energy at stagnation.

1. Introduction

Hot-spot ignition planned at the National Ignition Facility (NIF) [1] requires proper assembly of the fuel with an areal density (ρR) exceeding $\sim 1\,g\,cm^{-2}$ surrounding a ~5 keV hot spot with a ρR of $\sim 0.3\,g\,cm^{-2}$. Experimental information about the fuel assembly, as manifested by ρR and ρR asymmetries, and the hot-spot ion temperature (T_i) and yield (Y_n) are therefore critical for understanding the performance of an inertial confinement fusion (ICF) implosion. To obtain this information, a suite of neutron-time-of-flight (nTOF) spectrometers [2–4] and a magnetic recoil spectrometer (MRS) [4–7] have been commissioned and routinely used for measurements of the directional ICF neutron spectrum to an unprecedented accuracy in the energy range from 1.5 to 20 MeV. This range covers the essential details of the neutron spectrum, allowing for the determination of ρR, Y_n, and T_i. These spectrometers are fielded at different locations

around implosion to allow for measurements of the directional neutron spectrum from which ρR asymmetries and kinetic energy possibly remaining at nuclear burn can be determined. As discussed in this paper, these data have been essential to identifying key implosion-performance issues and to the progress towards the goal of achieving ignition for the first time in a laboratory [8].

The paper is structured as follows: section 2 describes the different components of the ICF neutron spectrum relevant to a cryogenically layered deuterium–tritium (dt) implosion at the NIF, and section 3 discusses the information carried by the neutron spectrum. Section 4 provides a short description of the neutron spectrometers installed on the NIF, as they have been discussed in more detail elsewhere [2–7], section 5 summarizes the neutron-spectrometry data obtained in different tuning campaigns and elaborates on some of the implications of the results in the context of achieving ignition. Section 6 discusses the path forward, and section 7 provides a short summary.

2. The ICF neutron spectrum

2.1. Primary neutrons

In a dt implosion, primary neutrons are produced primarily through the reaction

$$\mathrm{d} + \mathrm{t} \rightarrow {}^{4}\mathrm{He} + \mathrm{n} \qquad (Q = 17.59\ \mathrm{MeV}). \tag{1}$$

Here, Q is the difference in rest mass between the reactants and fusion products. For a zero-temperature plasma, the kinetic energy of the alpha particle and neutron is determined by the Q value and masses. For a plasma with a significant temperature, the kinetic energy of the reactants is not negligible relative to the Q value and must be considered when determining the energy of the neutron produced. The classical kinetic energy of the neutron (E_n) is then given by [9]

$$E_\mathrm{n} = \frac{1}{2} m_\mathrm{n} V_\mathrm{CM}^2 + \frac{m_\mathrm{n}}{m_\alpha + m_\mathrm{n}}(Q + K) + V_\mathrm{CM}\cos\theta \times \sqrt{\frac{2 m_\mathrm{n} m_\alpha}{m_\alpha + m_\mathrm{n}}(Q + K)}, \tag{2}$$

where m_n and m_α is the mass of the alpha particle and neutron, respectively, V_CM is the velocity of the centre-of-mass (CM) system, and K is the relative kinetic energy of the reactants. V_CM and K are given by

$$V_\mathrm{CM} = \frac{m_\mathrm{d} v_\mathrm{d} + m_\mathrm{t} v_\mathrm{t}}{m_\mathrm{d} + m_\mathrm{t}} \tag{3}$$

$$K = \frac{1}{2}\frac{m_\mathrm{d} m_\mathrm{t}}{m_\mathrm{d} + m_\mathrm{t}} v_\mathrm{rel}^2. \tag{4}$$

Here, m_d, m_t and v_rel is the deuteron mass, triton mass, and relative velocity of the reactants, respectively. The angle θ in the last term in equation (2) is defined as the angle between the direction of the V_CM vector and direction of the emitted neutron in the laboratory system. For a thermal plasma in which the distribution of the reactants and emission of neutrons are isotropic, the last term in equation (2) vanishes and the mean energy of the neutrons can be expressed as

$$\langle E_\mathrm{n}\rangle = E_0 + \frac{1}{2} m_\mathrm{n}\langle V_\mathrm{CM}^2\rangle + \frac{m_\mathrm{n}}{m_\alpha + m_\mathrm{n}}\langle K\rangle, \tag{5}$$

where E_0 is given by $m_\alpha Q/(m_\mathrm{n}+m_\alpha)$ and equal to 14.028 MeV (corrected for relativistic effects). As shown by equation (5), the mean energy of the emitted primary neutrons increases as the plasma temperature increases. For ICF plasmas, T_i/Q is $\sim 10^{-3}$, which introduces a systematic error in the neutron-mean energy when classical kinematics is used. As this error is about the same as the peak shift due to T_i (equation (5)), relativistic kinematics must be used to quantify the peak shift caused by T_i [10].

Kinetic energy of the main fuel, such as such as collective bulk motion, possibly remaining at nuclear burn adds an energy shift to the neutron-mean energy. This shift varies depending on the angle θ between the spectrometer line-of-sight (LOS) and direction of the bulk motion. To characterize the effect of the bulk velocity (V_bulk) on the observed primary-neutron spectrum, it is reasonable to assume that $K \ll Q$ and $V_\mathrm{bulk} \approx V_\mathrm{CM}$, which leads to the approximation [11]

$$\Delta E_\mathrm{bulk} \approx \frac{1}{2} m_\mathrm{n} V_\mathrm{bulk}^2 \cos^2\theta + V_\mathrm{bulk}\cos\theta \left[\frac{2 m_3 m_4}{m_3 + m_4} Q\right]^{\frac{1}{2}}. \tag{6}$$

For a spherical implosion, V_bulk is small, which means that the first term can be neglected, since it is about five orders of magnitude smaller than the second term. For bulk velocities approaching 1000 μm ns^{-1} both terms are comparable.

2.2. Down-scattered neutrons

In NIF implosions with a cryogenically layered dt fuel and a CH ablator, the fuel ρR typically exceeds 1 g cm^{-2} and the CH ablator approaches values of 0.4 g cm^{-2}. Under these conditions, a large fraction of the primary neutrons elastically scatter off the fuel and ablator ions as described by

$$\mathrm{n} + \mathrm{d} \rightarrow \mathrm{d}'(<12.5\ \mathrm{MeV}) + \mathrm{n}'(1.6 - 14.1\ \mathrm{MeV}) \tag{7}$$

$$\mathrm{n} + \mathrm{t} \rightarrow \mathrm{t}'(<10.6\ \mathrm{MeV}) + \mathrm{n}'(3.5 - 14.1\ \mathrm{MeV}) \tag{8}$$

$$\mathrm{n} + \mathrm{p} \rightarrow \mathrm{p}'(<14.1\ \mathrm{MeV}) + \mathrm{n}'(<14.1\ \mathrm{MeV}) \tag{9}$$

$$\mathrm{n} + {}^{12}\mathrm{C} \rightarrow {}^{12}\mathrm{C}'(<4.1\ \mathrm{MeV}) + \mathrm{n}'(2.1 - 14.1\ \mathrm{MeV}). \tag{10}$$

Here, the energy ranges of the reaction products are given in the parenthesis. As shown by these expressions, the scattering processes generate an energy continuum of neutrons. For energies in the range 10–12 MeV, the shape and magnitude of the scattered neutron spectrum is, to the first order, dictated by the differential cross sections for the n+d and n+t scattering processes, which are well known [12]. At lower energies, neutrons from break-up reactions and multiple scattering (MS) become more important and must be accounted for in the analysis of the spectrum (for equimolar dt fuel, the tt reaction is insignificant). Figure 1(*a*) illustrates the differential cross sections for n+t and n+d elastic scattering and the t(n,2n) and d(n,2n) reactions. For comparison, the level of MS is shown for a fuel ρR of 1 g cm^{-2}. This component, normalized to the single-scattering component defined by the sum of the n+d and n+t differential cross sections, was determined by HYDRA modelling [13] of a simple sphere consisting of 1 g cm^{-2} dt fuel. In figure 1(*b*), the differential cross sections for n+p

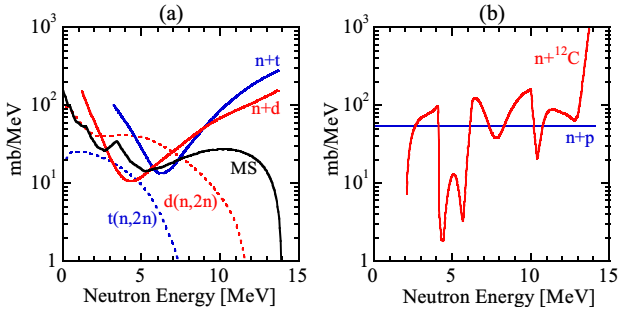

Figure 1. (*a*) The differential cross section for the n+t and n+d elastic scattering in addition to t(n,2n) and d(n,2n) break-up reactions. The multi-scattering (MS) component is also shown for a fuel ρR of 1 g cm^{-2}. This component is normalized to the single-scattering component, defined by the sum of the differential cross sections for the n+d and n+t elastic scattering processes. (*b*) The differential cross sections for the n+p elastic scattering, and n+^{12}C elastic and inelastic scattering. The elastic n+^{12}C scattering generates neutrons in the range 10–14 MeV, inelastic n+^{12}C scattering on the first, second and third excited state of ^{12}C generates neutrons in the energy range 6.3–9.5 MeV, 3.7–6.2 MeV and 2.1–4.1 MeV, respectively.

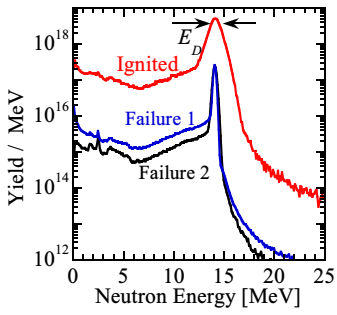

Figure 2. ICF neutron spectra simulated by LASNEX for three cryogenically layered dt implosions at the NIF. The spectrum marked red is for an ignited implosion, producing a neutron-burn averaged T_i of ∼40 keV and Y_n of 6×10^{18}. The spectra marked blue and black are produced by implosions that failed to ignite, generating a T_i of ∼5 keV and significantly lower Y_n. The 2.0 g cm^{-2} failure (electron-conduction issues) produces a significantly higher dsr component and a stronger thermal component than the 1.0 g cm^{-2} failure (entropy issues). Using the primary yield, the spectrum for failure 1 is normalized to the spectrum for failure 2 to illustrate the different levels of down-scattered neutrons relative to primary-neutron yield.

elastic scattering, n+^{12}C elastic and n+^{12}C inelastic scattering processes are shown [14, 15]. These processes must be taken into account in the analysis of the neutron spectrum if the ρR of the CH ablator is comparable or larger than the ρR of the dt fuel. The yield of the scattered neutrons in the energy range 10–12 MeV relative to Y_n, called the down-scattered ratio (dsr), is used as metric for determining the compression performance of NIF implosions. It is shown in section 3 that this parameter is, to the first order, proportional to the ρR for values below ∼0.5 g cm^{-2}. At higher ρR values, a second-order term needs to be added to account for the fact that MS removes a small fraction of the down-scattered (single scatter) from the energy range 10–12 MeV.

As discussed by Gatu Johnson [4], the part of the implosion probed by a single spectrometer depends on the energy range used for the dsr analysis of the neutron spectrum, composition of the fuel and ablator material, energy dependence of the differential cross section for the different nuclear processes shown in figure 1, and 3D structures in the implosion. Currently, the 10–12 MeV neutron-energy range is used for the dsr measurement, which corresponds to a relatively small portion of the implosion (∼20% coverage). To provide better coverage of the implosion and better measurement of the average dsr, a larger energy range needs to be used. Ultimately, the plan is to use the whole neutron spectrum down to thermal energies to extract as much information as possible about the implosion. In addition to using the complete neutron spectrum for diagnosing an implosion, the use of several neutron spectrometers with different LOS provide significantly better coverage and thus a better average measurement of the dsr. Another important advantage of multiple LOS is that dsr (or ρR) asymmetries can be accurately diagnosed, as discussed in sections 3.2 and 4.

2.3. Tertiary neutrons

A small fraction of the up-scattered deuterons (d′) or tritons (t′) produced in processes (7) and (8) undergo reactions with the thermal ions while traversing the fuel. These reactions produce tertiary neutrons (n'') as described by

$$\mathrm{d}'(<12.5\,\mathrm{MeV}) + \mathrm{t} \rightarrow {}^4\mathrm{He} + \mathrm{n}''(12.0 - 30.1\,\mathrm{MeV}) \quad (11)$$

$$\mathrm{t}'(<10.6\,\mathrm{MeV}) + \mathrm{d} \rightarrow {}^4\mathrm{He} + \mathrm{n}''(9.2 - 28.2\,\mathrm{MeV}). \quad (12)$$

The probability for generating tertiary neutrons above 20 MeV is proportional to ρR and ρR^2 for high-ρR and low-ρR implosions, respectively [16]. According to LASNEX simulations [17], the yield of tertiary neutrons is about 10^{-6} of Y_n. In addition to processes (11) and (12), tertiary neutrons are produced by the following process: dt alphas transfer several MeV to the thermal d's and t's by large angle Coulomb or nuclear-elastic scattering. These collisions give rise to non-thermal populations of d's and t's, which can in turn react with the thermal ions, generating an alpha-induced tertiary component in the neutron spectrum. Although produced at much lower yields than the primary-neutron component (∼10^{-6} to ∼10^{-3} depending on the implosion), this component typically dominates at energies in the range 16–20 MeV. However, this type of measurement has not yet been conducted and used for diagnosing cryogenically layered dt ICF implosions at the NIF because yields have been too low. Further discussions about the generation and use of the alpha-induced tertiary neutrons are found in the papers by Fisher *et al* [18], Ballabio *et al* [19] and Källne *et al* [20].

2.4. Simulated ICF neutron spectra

Figure 2 illustrates ICF neutron spectra simulated by LASNEX for three cryogenically layered dt implosions. These spectra are based on the reaction processes discussed in previous sub-section in addition to the dd and tt reactions, which produce neutrons with an average energy of 2.45 MeV and a continuum of neutrons up to 9.5 MeV, respectively. As shown in the figure, the width and magnitude of the primary-neutron spectrum marked red is substantially larger than the widths of the primary-neutron spectra produced in the failed implosions,

indicating a significantly higher T_i and Y_n, respectively. When contrasting the level of scattered neutrons in the range 10–12 MeV and thermal neutrons below 1 MeV, it is also clear that higher ρR is achieved in failure 1 (electron conduction failure) than in failure 2 (entropy failure). At neutron energies above 16 MeV, the effects of alpha-induced and neutron-induced tertiary reactions start to become apparent.

3. Information carried by the ICF neutron spectrum

3.1. 1D implosion parameters—Y_n, T_i and ρR

As alluded to in section 2, the primary neutrons carry a wealth of information about the implosion. As shown by Brysk for a thermal plasma [9], T_i can be determined from the width (ΔE_D) of the Doppler broadened primary neutron spectrum, as described by

$$T_i = \frac{m_\alpha + m_n}{16 \ln 2 m_n \langle E_n \rangle} \Delta E_D^2. \quad (13)$$

Y_n is determined from the primary peak by integrating the spectrum from 13 to 15 MeV. For more detailed discussions about what information can be determined from primary-neutron spectrum, the reader is referred to the papers by Brysk [9], Ballabio *et al* [10] and Appelbe *et al* [21]. As discussed by Appelbe, additional broadening may arise from residual fuel kinetic energy during burn, which is 3D in nature. This effect manifests itself as a deviation from a single-Gaussian primary-neutron spectrum characterized by the neutron-mean energy and T_i. Both the shape and average energy of the primary-neutron spectrum are affected by residual fuel-kinetic energy possibly remaining during burn. From equation (6), one can compute that a V_{bulk} of 200 μm ns^{-1} corresponds to a mean energy shift of about 100 keV. Quantifying the effect of residual kinetic energy on the shape and average energy of the primary-neutron spectrum is a non-trivial task and outside the scope of this paper, but will be subject to future studies [22].

The down-scattered neutron spectrum provides 1D information about the fuel assembly. From the measured dsr, a ρR value can be inferred by using a relatively simple model of an implosion (hot-spot model). In this model, where all neutrons are produced in the centre of a spherically symmetric implosion, the total ρR consisting of both dt fuel and CH ablator is related to the measured dsr ($\mathrm{dsr_{dt}}$ + $\mathrm{dsr_{CH}}$) in the energy range E_1–E_2 by

$$\rho R = \rho R_{dt} + \rho R_{CH} = \int_{E_1}^{E_2} \left(\frac{(2\alpha + 3)\, m_p}{\alpha \sigma_{nd}(E) + \sigma_{nt}(E)} \mathrm{dsr_{dt}}(E) + \frac{(\beta + 12) m_p}{\beta \sigma_{np}(E) + \sigma_{n^{12}C}(E)} \mathrm{dsr_{CH}}(E) \right) \mathrm{d}E. \quad (14)$$

Here, m_p is the proton mass, $\sigma_{nd}(E)$, $\sigma_{nt}(E)$, $\sigma_{np}(E)$ and $\sigma_{n^{12}C}(E)$ is the n+d, n+t, n+p and n+^{12}C differential cross section for single scattering, respectively. For an equimolar dt fuel and CH ablator, $\alpha = n_d/n_t = 1$ and $\beta = n_p/n_c = 1$. As σ_{DT}(10–12 MeV) and σ_{CH}(10–12 MeV) is about 400 mb and 120 mb, respectively, and $\sigma_{dt}(E) = \sigma_{nd}(E) + \sigma_{nt}(E)$, and $\sigma_{CH}(E) = \sigma_{np}(E) + \sigma_{n^{12}C}(E)$, equation (14) can be approximated by

$$\rho R = \rho R_{dt} + \rho R_{CH} \approx 21\, \mathrm{dsr_{dt}} + 179\, \mathrm{dsr_{CH}} (g\ \mathrm{cm}^{-2}). \quad (15)$$

Equation (15) indicates that the scattered neutrons probe primarily ρR_{dt} and are relatively insensitive to the ρR_{CH} due to different interaction probabilities per unit ρR. According to LASNEX simulations, the ρR_{CH} is also small in comparison to ρR_{dt} (about 10–20%), allowing the second term in equation (15) to be neglected when inferring ρR from the measured neutron spectrum. However, since the total ρR sets the confinement time of the hot spot [23], it is also important to determine ρR_{CH}. Other measurement techniques have therefore been proposed and are currently being implemented for diagnosing ρR_{CH} [24, 25]. It should be noted that equation (15) is valid for ρR values up to about 0.5 g cm^{-2} when MS can be neglected. At higher values, MS must be considered for a better determination of the ρR_{dt}. Using HYDRA modeillng of a simple sphere consisting of dt fuel with a ρR_{dt} varying from 0.2 to 2.0 g cm^{-2}, it was established that a second-order term needs to be added to the linear ρR-dsr relationship for the fuel to account for the effect of MS[7], i.e,

$$\rho R_{dt} \approx 21\, \mathrm{dsr_{dt}} + 80\, \mathrm{dsr_{dt}^2}\ (\mathrm{g\,cm^{-2}}). \quad (16)$$

This expression is valid for ρR_{dt} values up to ~2 g cm^{-2} when shadow effects between individual scattering processes start to become important. To account for this effect third-order term needs to be added to equation (16).

A more realistic 1D representation of ρR_{dt} can be determined from the measured dsr by considering the effect of the spatial birth profile of primary neutrons and profile of the high-density region. As an implosion can be approximated by a low-density central hot spot surrounded by a high-density fuel shell, it is reasonable to assume that most ρR_{dt} is positioned between the radii R and $R + \delta R$, where R represents the radius of the hot spot (or primary source) and δR represents the thickness of the high-density fuel shell. When considering a parabolic primary-source profile that extends to radius R, and a constant-density fuel shell between R and $R+\delta R$, equation (16) can be approximated by the expression

$$\rho R_{dt} \approx \left(21\, \mathrm{dsr_{dt}} + 80\, \mathrm{dsr_{dt}^2}\right) \left(1 - \frac{0.17}{1 + \frac{\delta R}{R}}\right). \quad (17)$$

The geometric factor takes into account that the average path length of the primary neutrons is longer than the radial distance through the high-density fuel shell. In the limiting case of the hot-spot model ($R = 0$), equation (17) is identical to the first term of equation (15). To accurately determine the effect of the implosion geometry on the ρR determination, R and δR must be measured. This is done with neutron and x-ray imagining techniques [26, 27].

3.2. 3D structures—low-mode ρR asymmetries

Low-mode ρR asymmetries in the fuel can be determined from the complete spectrum of down-scattered neutrons by correlating different energy ranges to different portions of the implosion. This is possible because the energy of the down-scattered neutron depends on the scattering angle in the case

[7] HYDRA modelling of simple a sphere with a fuel ρR varying in the range 0.2–2.0 g cm^{-2} was used to establish the linear behaviour of the ρR (dsr) function for values below 0.5 g cm^{-2} and slightly non-linear behaviour for values larger than 0.5 g cm^{-2}. The non-linear behaviour is represented by the 2nd-order term in equation (16).

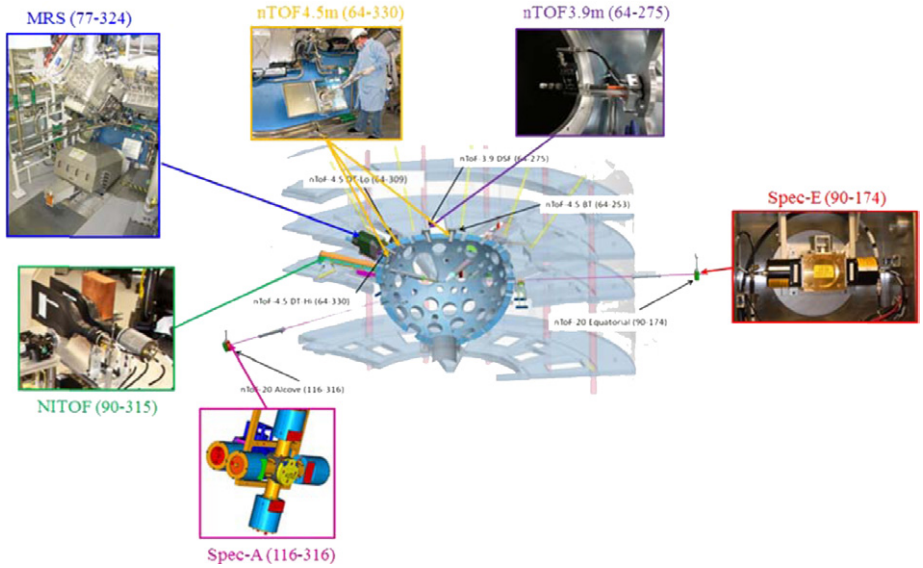

Figure 3. A cut-through image of the NIF target chamber, illustrating the locations of the MRS and nTOF spectrometers used for measurements of the directional ICF neutron spectrum, from which Y_n, T_i and ρR and ρR asymmetries are determined.

of n+d and n+t scattering or production angle in the case of d(n,2n) and t(n,2n) reactions shown in figure 1. Mapping out the ρR asymmetries from the down-scattered neutron spectrum is, however, complicated and requires detailed information about size, shape and absolute locations of the primary-neutron source and high-density fuel shell. A conceptually more powerful method for diagnosing ρR asymmetries is to measure the directional neutron spectrum at various locations around the implosion. This type of measurement puts stringent constraints on the modelling of the implosion, in terms of characterizing ρR asymmetries and possible fuel-shell kinetic energy remaining at burn and stagnation.

Understanding the origin of ρR asymmetries is an essential prerequisite for achieving ignition because non-spherical assembly of the main fuel can reduce the efficiency of converting shell kinetic energy to hot-spot thermal energy at stagnation, possibly leading to lower hot-spot pressure and reduced confinement [28]. In recent years, the increasing availability of 3D simulation tools (e.g., HYDRA) has made it possible to computationally assess the impact of 3D effects on the implosion dynamics and experimental observables [29]. While progress has been made in developing 3D modelling capabilities, ongoing development is still required to build an extensive data base for validating and improving numerical modelling. Semi-analytical 3D modelling is also being implemented, in which an implosion model based on spherical harmonics is adjusted until the best match to the experimental observations (both nuclear and x-ray signatures) is found [30, 31].

4. Neutron spectrometry on the NIF

A suite of twelve nTOF spectrometers and an MRS have been commissioned and used extensively for measurements of the ICF neutron spectrum at the NIF to an unprecedented accuracy in the energy range from 1.5 to 20 MeV [4]. This range covers the essential details of the neutron spectrum, allowing for the determination of dsr (or ρR), Y_n, and T_i. The spectrometers are fielded at different locations around the implosion for directional measurements of the spectrum, also allowing for determination of ρR asymmetries and possible fuel-shell kinetic energy remaining at nuclear burn and stagnation. Figure 3 shows the locations of the different spectrometers around the NIF target chamber. The suite of nTOF spectrometers consists of the Spec-A (116°–316°) and Spec-E (90°–174°), both positioned at about 20 m from TCC, the chemical vapour deposition (CVD) diamond (64°–275°) positioned at 3.9 m, the NITOF plastic scintillator (90°–315°) at 27.3 m, and the set of plastic scintillators at 4.5 m (nTOF4.5 m). All nTOFs consist of either a fast CVD diamond or a scintillator detector coupled to a photodiode (PD) or photomultipler tube (PMT) biased to high voltage. Each nTOF is operated in current mode with the signal collected on one or more oscilloscopes. With a fixed and known distance to TCC and known spectrometer response function, the neutron spectrum can be inferred from the nTOF signal. The MRS, which is based on an entirely different concept, consists of four components: a deuterated polyethylene foil (CD_2) positioned 26 cm from TCC, a focusing magnet positioned outside the NIF target chamber, an array of nine CR-39 detectors positioned at the focal plane of the spectrometer, and 6000 lbs of polyethylene shielding enclosing the spectrometer. The operating principle of the MRS is as follows: a small fraction of the emitted neutrons hit the CD_2 foil and produce elastically scattered deuterons. Forward-scattered deuterons are selected by a magnet aperture positioned in front of the magnet. These deuterons are momentum analysed and focused onto the array of CR-39 detectors. The energy of the deuteron is determined from the position of the detected deuteron. The CR-39 detectors are removed from the MRS and processed in an etch and scan lab, and then analysed to reconstruct the recoil deuteron spectrum, from which the neutron spectrum is inferred. For further details and more in-depth discussions of the nTOF and MRS spectrometers, the reader is referred to [2–7].

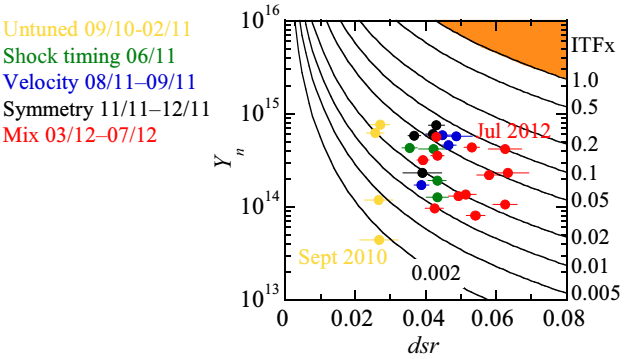

Figure 4. Measured Y_n (DT equivalent) as a function of measured dsr. Each solid curve represents a constant *ITFx* value. The orange region represents the plasma conditions at which there is at least a 50% probability for achieving ignition according to simulations. Neutron-spectrometry data obtained in five campaigns are shown, which indicate that the ITFx has improved almost two orders of magnitude since the first shot taken in September 2010. The untuned implosions are shown in light orange; post-shock timing implosions with germanium doped CH ablators are shown in green; high velocity implosions with silicon doped CH ablators are shown in blue; implosions with spherical shape tuning are shown in black; and the implosions with both nominal and extended pulse with silicon doped CH ablators for exploring the mix-performance cliff are shown in red.

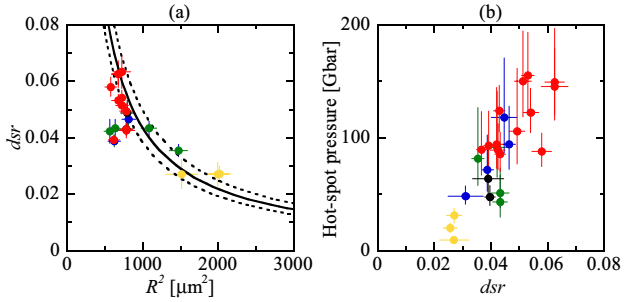

Figure 5. (*a*) Dsr as a function of R^2, where R represents the radius of the hot spot determined from neutron and/or x-ray imaging measurements. (*b*) Modelled hot-sport pressure as function of dsr. The maximum hot-spot pressure is almost a factor of two less than the point design. The colour scheme is the same as in figure 4.

5. Neutron-spectrometry data and discussion

One metric for characterizing the implosion performance is the experimental ignition threshold factor (ITFx), which is used for identifying key-physics issues and for guiding the experimental campaign towards the conditions required for ignition. As described by Edwards *et al*, Glenzer *et al* and Spears *et al* [8, 32, 33], the ITF*x* depends on Y_n and dsr as expressed as

$$\mathrm{ITFx} = \left(\frac{Y_n}{3\times 10^{15}}\right)\left(\frac{\mathrm{dsr}}{0.07}\right)^{2.3}. \qquad (18)$$

The advantage of using the ITFx formalism is that it allows for direct use of the measured implosion parameters. Y_n provides information about the hot-spot formation and dsr provides information about the assembly of the main fuel. For convenience, the ITFx parameter has been normalized to one where the probability of achieving ignition is 50%. According to simulations, the yield enhancement from alpha-energy deposition exceeds the yield from compression alone for ITFx values in the range 0.3–0.5. Figure 4 shows observed Y_n as a function of dsr for the campaigns conducted to date. The solid curves represent *ITFx* values ranging from 2×10^{-3} to 1, and the orange area indicates the conditions required for ignition, according to simulations. As shown by figure 4, significant improvement in *ITFx* for the untuned implosions (marked orange) was achieved between the first implosion conducted in September 2010 and February 2011 [34]. This improvement, mostly in the Y_n, was realized by increasing the laser power, initial shock tuning, and improvements of the hohlraum to prevent frozen condensation from freezing on the laser entrance–hole windows. In the next three tuning campaigns, the neutron data indicate an ITFx increase to ~0.08. This was achieved primarily with improved shock timing [35], increased implosion velocity using Si-doped CH ablators, increased laser performance, and improved implosion symmetry. In the Mix campaign, the rate of rise of the fourth pulse was decreased, producing an implosion that could reach higher compression and lower adiabat. The length of the pulse was also extended to prevent decompression of the fuel shell during the coasting phase. This resulted in the highest achieved dsr of ~0.063 and ITFx of ~0.1 at significantly lower velocities and decreased drive energy. Even though the ITFx has improved almost two orders of magnitude since the first shot taken in September 2010, the observed Y_n are found to be 3 to 10 times lower than post-shot HYDRA and LASNEX simulated yields. Figures 5(*a*) and (*b*) illustrate the improved implosion performance in terms of dsr versus the square of the hot-spot radius, and inferred hot-spot pressure versus dsr. The hot-spot radii were determined from images of the primary-neutron source and the hot-spot pressure was determined from 3D semi-analytical modelling and numerical simulations of the implosions that generate results consistent with the observables [31, 36]. As shown by figures 5(*a*) and (*b*), an improved convergence was achieved throughout the tuning campaigns, resulting in higher dsr values and hot-spot pressures. The maximum dsr achieved is ~85% of that specified for the point design. The solid curve represents the scaling between dsr and R^2 using a simple 1D implosion model given by $\mathrm{dsr} \propto m_{\mathrm{fuel}}/[4\pi R^2(1+\delta R/2R)^2]$, while the dashed curves represent the uncertainty associated with the scaling. As discussed in section 3.1, δR represents the thickness of the high-density fuel shell. A $\delta R/R$ value of 0.5 ± 0.2 determined from neutron and x-ray images was used in this modeling. According to the semi-analytical modelling of the experimental observables and numerical simulations, a maximum hot-spot pressure of ~150 Gbar was achieved in the Mix campaign. This is almost a factor of two lower than the conditions required for ignition, according to simulations. This pressure deficit probably explains the lower observed yields than predicted.

A potential source for the observed pressure deficit is low-mode ρR asymmetries generally observed in the implosions. From the down-scattered neutron yields in the 10–12 MeV range as measured by the Spec-A and Spec-E nTOFs and MRS, which have different LOS, the presence of large low-mode ρR asymmetries was determined. Figure 6 shows the dsr asymmetries observed by the MRS and Spec-E nTOF

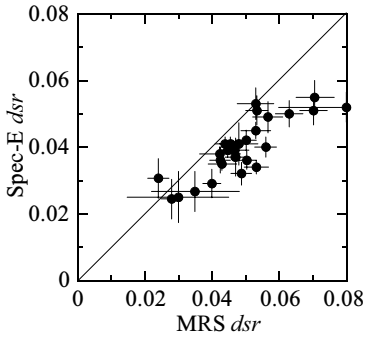

Figure 6. Dsr measured by MRS and Spec-E nTOF for all cryogenically layered dt shots to date. The dsr was determined from measurements of down-scattered neutrons in the range 10–12 MeV, which corresponds to a small portion of the implosion (∼20%). These spectrometers are positioned close to the equator almost diametrically opposite of each other. The observed dsr (or ρR) asymmetries, which are substantial, may contribute to the lower than predicted pressures and Y_n.

when measuring down-scattered neutrons in the range 10–12 MeV, which corresponds to a small portion of the implosion. These low-mode ρR asymmetries, possibly, caused by drive asymmetries or initial capsule imperfections may lead to less efficient transfer of the shell kinetic energy to thermal hot-spot energy and potentially enhancing fuel-ablator mix, as discussed by Thomas and Kares [37]. Indeed, the 3D modelling of the isobaric pressure suggests that more than 50% of the available kinetic energy is not being coupled to the hot spot [31].

6. Path forward

It is probable that the observed low-mode ρR asymmetries have a detrimental impact on the fuel assembly and hot-spot formation and on current attempts to achieve ignition. A quantitative understanding of the various sources of asymmetry is therefore required to achieve progress in optimizing ignition platforms. Since many of the potential sources of asymmetry are 3D in nature, the goal should be to develop an experimental data base that can be used to validate and improve the modelling capabilities as they mature, particularly since robust 3D computing is still in its infancy. As a first step, lower CR implosions, more 1D in nature, should be examined and understood as a stepping-stone to improving the modelling capabilities before conducting the high-convergence implosions necessary for ignition.

7. Summary

Neutron-spectrometry data, obtained with the MRS and nTOFs on the NIF, have been essential to identifying key issues with the cryogenically layered dt implosions and for guiding experimental campaign at the NIF towards the conditions required for ignition. The data indicate that the implosion performance, characterized by ITFx, has improved almost two orders of magnitude since the first shot taken in September 2010. ρR values greater than $1\,\mathrm{g\,cm^{-2}}$ are now readily achieved. 3D semi-analytical modelling of the neutron-spectrometry data, as well as other data, indicate that a maximum hot-spot pressure of ∼150 Gbar has been achieved, which according to HYDRA simulations is almost a factor of two below conditions required for ignition. The conjecture is that the pressure deficit, which could explain the 3–10 times lower observed Y_n than predicted, is partly explained by low-mode ρR asymmetries generally observed in cryogenically layered dt implosions.

References

[1] Miller G.H. *et al* 2004 The National Ignition Facility: ushering in a new age for high energy density science *Nucl. Fusion* **44** S228
[2] Glebov Yu.V. *et al* 2010 The National Ignition Facility neutron time-of-flight system and its initial performance *Rev. Sci. Instrum.* **81** 10D325
[3] Moran M.J. *et al* 2012 Deuterium–tritium neutron yield measurements with the 4.5 m neutron-time-of-flight detectors at NIF *Rev. Sci. Intrum.* **83** 10D213
[4] Gatu Johnson M. *et al* 2012 Neutron spectrometry—an essential tool for diagnosing implosions at the National Ignition Facility *Rev. Sci. Instrum.* **83** 10D308
[5] Frenje J.A. *et al* 2001 A neutron spectrometer for precise measurements of DT neutrons from 10 to 18 MeV at OMEGA and the National Ignition Facility *Rev. Sci. Instrum.* **72** 854
[6] Frenje J.A. *et al* 2008 First measurements of the absolute neutron spectrum using the magnetic recoil spectrometer at OMEGA *Rev. Sci. Instrum.* **79** 10E502
[7] Frenje J.A. *et al* 2010 Probing high areal-density cryogenic deuterium–tritium implosions using downscattered neutron spectra measured by the magnetic recoil spectrometer *Phys. Plasmas* **17** 056311
[8] Edwards M.J. *et al* 2011 The experimental plan for cryogenic layered target implosions on the National Ignition Facility—the inertial confinement approach to fusion *Phys. Plasmas* **18** 051003
[9] Brysk H. 1973 Fusion neutron energies and spectra *Plasma Phys.* **15** 611
[10] Ballabio L. *et al* 1998 Relativistic calculation of fusion product spectra for thermonuclear plasmas *Nucl. Fusion* **38** 1723
[11] Tardocchi M. *et al* 2004 Ion temperature and plasma rotation profile effects in the neutron emission spectrum *Rev. Sci. Instrum.* **75** 661
[12] Frenje J.A. *et al* 2011 Measurements of the differential cross sections for the elastic n-^{3}H and n-^{2}H scattering at 14.1 MeV by using an inertial confinement fusion *Phys. Rev. Lett.* **107** 122502
[13] Marinak M.M. *et al* 2001 Three-dimensional HYDRA simulations of National Ignition Facility targets *Phys. Plasmas* **8** 2275
[14] Allred J.C. *et al* 1953 The interaction of 14-MeV neutrons with protons and deuterons *Phys. Rev.* **91** 90
[15] Dave J.H. *et al* 1983 Optical model analysis of scattering of 7- to 15-MeV neutrons from 1-*p* shell nuclei *Phys. Rev.* C **28** 2212
[16] Petrasso R.D. *et al* 1996 Measuring implosion symmetry and core conditions in the National Ignition Facility *Phys. Rev. Lett.* **77** 2718
[17] Fisher R. *et al* 1994 Fast alpha particle diagnostics using knock-on ion tails *Nucl. Fusion* **34** 1291
[18] Ballabio L. *et al* 1997 α-particle knock-on signature in the neutron emission of DT plasmas *Phys. Rev.* E **55** 3358
[19] Källne J. *et al* 2000 Observation of the alpha particle 'knock-on' neutron emission from magnetically confined DT fusion plasmas *Phys. Rev. Lett.* **85** 1246
[20] Zimmerman G.B. *et al* 1975 Numerical simulations of laser-initiated fusion *Comments Plasma Phys. Control. Fusion* **2** 51–61

[21] Appelbe B. *et al* 2011 The production spectrum in fusion plasmas *Plasma Phys. Control. Fusion* **53** 045002
[22] Gatu Johnson M. *et al* 2013 Observations of residual kinetic effects remaining at burn through measurements of spectral shifts in the primary neutron spectrum *Phys. Plasmas* submitted
[23] Betti R. *et al* 2010 Thermonuclear ignition in inertial confinement fusion and comparison with magnetic confinement *Phys. Plasmas* **17** 058102
[24] Frenje J.A. *et al* 2009 Diagnosing ablator ρR and ρR asymmetries in capsule implosions using charged-particle spectrometry at the National Ignition Facility *Phys. Plasmas* **16** 022702
[25] Herrmann H.W. *et al* 2010 Diagnosing inertial confinement fusion gamma ray physics *Rev. Sci. Instrum.* **81** 10D333
[26] Merrill F.E. *et al* 2012 The neutron imaging diagnostic at NIF *Rev. Sci. Instrum.* **83** 10D317
[27] Glenn S.M. *et al* 2012 Extracting core shape from x-ray images at the National Ignition Facility *Rev. Sci. Instrum.* **83** 10E519
[28] Goldstein W. *et al* 2012 *Report on Science of Fusion Ignition on NIF* LLNL-TR-570412
[29] Jones O.S. *et al* 2012 3D simulations of the NIF indirect drive ignition target design *J. Phys.* **244** 022077
[30] Springer P.T. *et al* 2012 Integrated thermodynamic model for ignition target performance *IFSA: Proc. for the Inertial Confinement Fusion Science and Applications Conf. (Bordeaux, France, 2011)*
[31] Cerjan C. *et al* 2013 Integrated diagnostic analysis of ICF capsule performance, accepted for publication *Phys. Plasmas* submitted
[32] Glenzer S.H. *et al* 2012 Cryogenic thermonuclear fuel implosions on the National Ignition Facility *Phys. Plasmas* **19** 056318
[33] Spears B. *et al* 2012 Performance metrics for inertial confinement fusion implosions: aspects of the technical framework for measuring progress in the National Ignition Campaign *Phys. Plasmas* **19** 056316
[34] Mackinnon A.J. *et al* 2012 Assembly of high-areal-density deuterium–tritium fuel from indirectly driven cryogenic implosions *Phys. Rev. Lett.* **108** 215005
[35] Robey H.F. *et al* 2012 Precision shock tuning on the National Ignition Facility *Phys. Rev. Lett.* **108** 215004
[36] Jones O.S. *et al* 2012 A high-resolution integrated model of the National Ignition Campaign cryogenic layered experiments *Phys. Plasmas* **19** 056315
[37] Thomas V.A. and Kares R.J. 2012 Drive asymmetry and the origin of turbulence in an ICF implosion *Phys. Rev. Lett.* **109** 075004